Volume 139 | Number 19 | 7 October 2014 | Pages 4719–5036

# Analyst

www.rsc.org/analyst

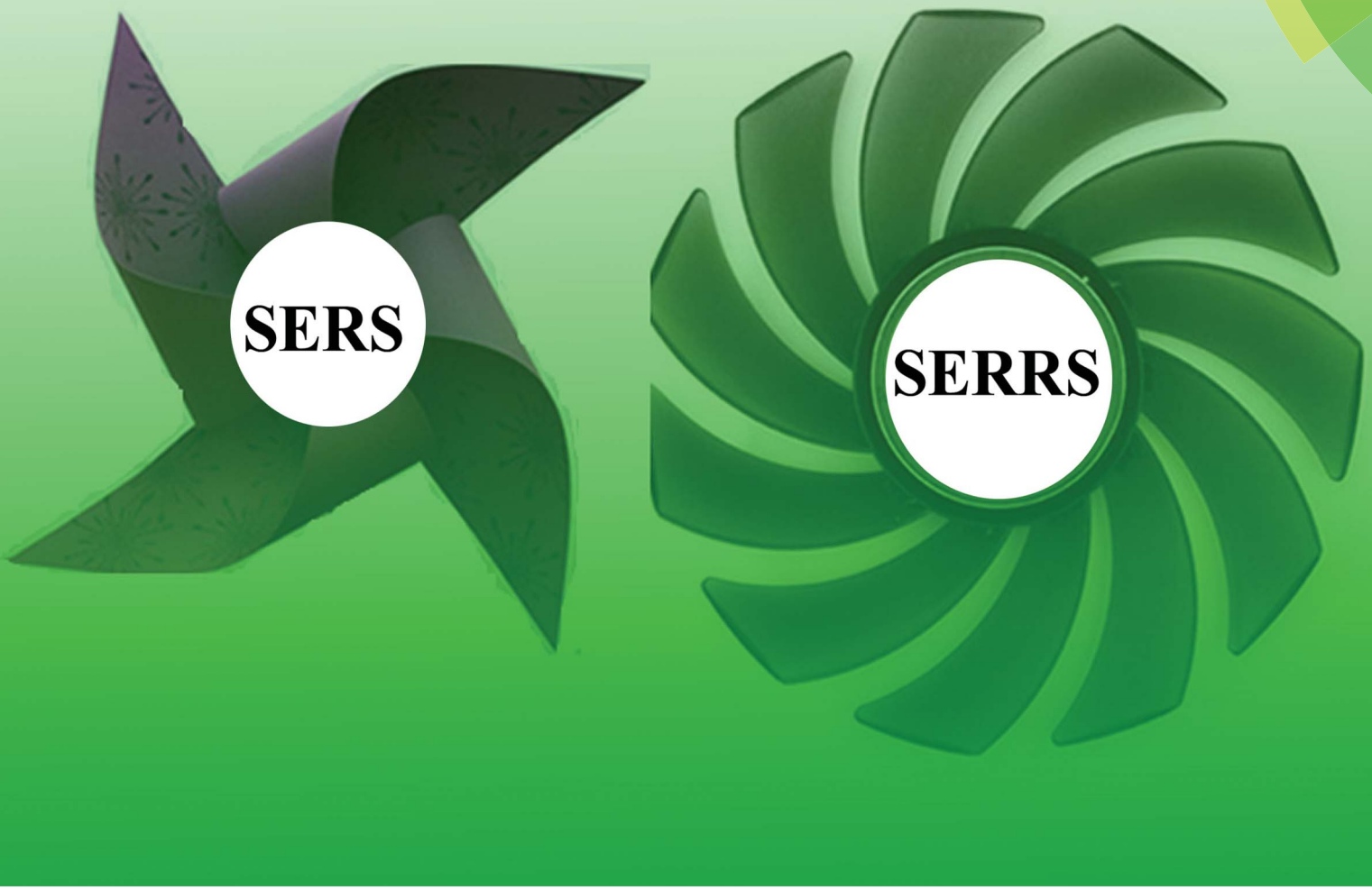


ISSN 0003-2654

ROYAL SOCIETY OF CHEMISTRY

PAPER

Liangbao Yang, Jinhuai Liu *et al.*

Designing and fabricating double resonance substrate with metallic nanoparticles–metallic grating coupling system for highly intensified surface-enhanced Raman spectroscopy

Analyst

PAPER

View Article Online
View Journal | View Issue

Cite this: *Analyst*, 2014, **139**, 4799

# Designing and fabricating double resonance substrate with metallic nanoparticles–metallic grating coupling system for highly intensified surface-enhanced Raman spectroscopy†

Ying Zhou,‡[ab] Xuanhua Li,‡[a] Xingang Ren,[c] Liangbao Yang*[ab] and Jinhuai Liu*[a]

Received 24th March 2014
Accepted 15th May 2014

DOI: 10.1039/c4an00540f

www.rsc.org/analyst

Recently, nanoparticle–film coupling systems in which metal nanoparticles (supported localized surface plasmons, LSPs) are separated from a flat metal film (supported surface plasmon polaritons, SPPs) by a spacer have been widely reported due to its strong local enhancement field. However, there is are limited studies, which employ the design of combing metal grating into the nanoparticle–film gap system. Here, we propose and fabricate a novel double-resonance SERS system by strategically assembling Au NPs separated by a $MoO_3$ nanospacer from an Ag grating film. The Ag grating with clear SPP effect is used for the first time in a double-resonance system, and the monolayer Au NPs array is well assembled onto the top of the Ag grating with a compact and uniform distribution (inter-particles gap of about 5 nm). As a result, we experimentally and theoretically demonstrate a significant near-field enhancement. The very strong near-field produced in the proposed SERS substrates is due to multiple couplings, including the Au NPs–Ag grating film coupling and Au NPs–Au NPs coupling. In addition, the as-proposed SERS substrates show good reproducibility of SERS, which have potential applications in plasmonic sensing and analytical science.

## Introduction

Surface-enhanced Raman scattering (SERS) has been a promising and powerful analytical technique since its discovery.[1,2] It refers to the phenomenon whereby Raman scattering is significantly enhanced when molecules are adsorbed on metallic nanostructures.[3] There have been many debates regarding its origin, whether it is electromagnetic or chemical. According to the widely accepted view, SERS is mainly caused by electromagnetic contribution.[4–7]

Surface plasmons (SPs) are the collective oscillation of electrons at the boundaries between materials and are often categorized into two classes, namely, surface plasmon polaritons (SPPs) and localized surface plasmons (LSPs).[8] SPPs are propagating electromagnetic waves bound to the interfaces between metals and dielectrics. They can be excited on a metal surface by prism coupling or grating coupling over a large range of frequencies. On the other hand, LSPs are non-propagating excitations of the electrons in metal nanoparticles (NPs), which are much smaller than the incident wavelength. The LSP resonance properties of a metal nanoparticle depend on its size, shape, and the permittivity and dielectric environment.[9] These phenomena can lead to a strong electromagnetic field enhancement near the surfaces of the nanostructure, where they have been employed for SERS.[10–18] Theoretical studies have predicted that strong coupling between LSPs and SPPs occurs when their resonance frequencies are approximately equal to each other.[19–22]

Recently, the nanoparticle–film coupling systems in which metal nanoparticles (supported localized surface plasmons, LSPs) are separated from a flat metal film (supported surface plasmon polaritons, SPPs) by a spacer have been widely reported due to its strong local enhancement field. One of the interesting features of NPs–film coupling configuration is that they are compatible, for most of its construction, which can be popularly adopted in most typical analytical sciences and related fields, such as surface-enhanced Raman scattering (SERS), surface-enhanced fluorescence spectra, and other plasmonic sensing with the requirements of large area and great spot-to-spot uniformity.[23–26] In the work of Chu,[23] the design included a metallic nano-disk array separated from a gold film

[a]*Institute of Intelligent Machines, Chinese Academy of Sciences, Hefei, 230031, China. E-mail: lbyang@iim.ac.cn; jhliu@iim.ac.cn; Fax: +86 551-5592420*

[b]*School of Chemistry and Chemical Engineering, Anhui University, Hefei, 230039, China*

[c]*Key Lab of Intelligent Computing and Signal Processing, Anhui University, Hefei, 230039, China*

† Electronic supplementary information (ESI) available: Typical higher-magnification TEM images and the specific measurements of Au NPs gap distance distribution of inter-particle separations. See DOI: 10.1039/c4an00540f

‡ Ying zhou and Xuanhua Li contributed equally to this work.

by a dielectric spacer. The SPP on the gold film interacted with the LSPR of the metallic array, and double resonance characteristics were observed in optical transmission measurements. In the work of Banaee,[24] "in-plane" nano-particle pairs were used to obtain plasmonic coupling.

Metal grating structure is a well-known structure, which shows efficient SPP. There are numerous reports on taking the advantage of SPP effect from metal grating for applications in plasmonic sensing and analytical science. Unfortunately, there are just a handful of reports on the studies of the double plasmonic effect given off by metal NPs supported by metal grating structures. In this work, we propose and fabricate a novel double-resonance SERS system by strategically assembling Au NPs separated by a $MoO_3$ nanospacer from an Ag grating film. The Ag grating showing clear SPP effect is used for the first time in a double-resonance system, and the monolayer Au NPs array is well assembled onto the top of the Ag grating with a compact and uniform distribution (inter-particles gap about 5 nm). As a result, we experimentally and theoretically demonstrate a significant near-field enhancement (the experimental enhancement factor reaches $2.47 \times 10^7$, which is one of the highest reported for the double-resonance system to date). The very strong near-field enhancement produced in the proposed SERS substrates is due to multiple couplings, including the Au NPs–Ag grating film coupling and Au NPs–Au NPs coupling. In addition, the as-proposed SERS substrates show good reproducibility of SERS, which will have potential applications in plasmonic sensing and analytical science.

## Experimental

### Synthesis of SERS substrates

1. Fabrication of Ag grating: PDMS, prepared by mixing an oligomer (Silard 184, Dow Corning) and a curing agent (10 : 1, v/v), was poured onto the silicon nanograting master. After removing the air bubbles and thermally curing at 79 °C for 3–4 h, PDMS molds were obtained in which the grating of the periodic nanostructures corresponded to the dimension of the master grating. Silver (80 nm) layers and $MoO_3$ spacer with different thicknesses were thermally evaporated in a stepwise manner onto the PDMS grating mold under vacuum at $10^{-6}$ Torr.

2. Fabrication of Au NPs: the synthesis of Au NPs was performed using the chemical reduction of chloroauric acid with sodium citrate method introduced by Frens.[27] $HAuCl_4$ solution (1.0 mL, 1.0 wt%) was mixed with water (99.0 mL) and heated to its boiling point. Upon boiling, trisodium citrate tetrahydrate (1.3 mL, 1.0 wt%) was added quickly to induce particle formation during prolonged heating under reflux for 30 min. The Au NPs with a diameter of 25 nm were obtained. The synthesis of Au monolayer film followed the gold nanoparticle assembly approach previously developed by Zhou.[28] A solution of $1 \times 10^{-6}$ M mPEG-SH in deionized water was first prepared. An appropriate polymeric solution was added to $2.94 \times 10^{-6}$ M of colloidal Au NPs. The sample was maintained for about 8 h at room temperature with stirring. Finally, the solution was assembled onto a substrate, and closely-packed NPs could be easily obtained.

### SERS and Raman experiments

The SERS data was collected on a LabRAM HR800 confocal microscope Raman system (Horiba JobinYvon) using a He–Ne ion laser operating at 632.85 nm. The laser beam was focused on the sample of the size of about 1.5 μm using a ×50 LMPLFLN microscope objective. The laser power was approximately 1 mW, and the integration time was 1 s for each spectrum. The data was collected with the same accumulation and integration times for all the samples. We dripped the crystal violet (CV) solutions on the substrates, and after they were dry, the substrates were subjected to SERS measurements. We collected SERS spectra from several randomly selected positions on the substrates.

### Theoretical modeling

Maxwell's equations were rigorously solved by utilizing the finite-difference time-domain (FDTD) method to better understand the nature of the strong near-field enhancement in the Au NPs–Ag grating coupling system.[29,30] In this modeling, the sample geometries closely matched those of the actual experimental samples, *i.e.*, a 25 nm Au NP on an Ag grating with a 350 nm period separated by a $MoO_3$. The thickness of $MoO_3$ was tuned from 2 nm, 15 nm, 30 nm, and 70 nm, respectively. The gap between the neighboring Au NPs was about 5 nm. The complex dielectric constant of metallic Au was taken from Johnson and Chrity.[31]

## Results and discussion

### Design and fabrication of double resonance substrate

A schematic diagram of the double resonance SERS substrate is shown in Scheme 1. It consists of a gold nanoparticle array, a $MoO_3$ spacer and a continuous silver grating film. PDMS mold was first prepared, followed by the thermal evaporation of silver layers and $MoO_3$ spacer onto the PDMS grating mold in a stepwise manner. The period of grating is 350 nm, as shown in Fig. 1A. Considering that the local field enhancement of hot spots is critically sensitive to the spacer between the

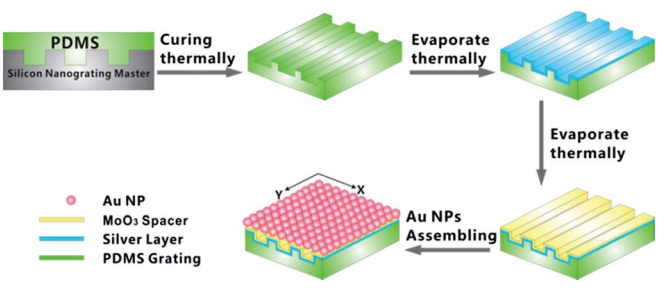


Scheme 1 Schematic representation of the synthesis of Au NPs/$MoO_3$/Ag grating double resonance substrate. Actual device has hundreds of periods along *x* and *y* axes; only a small portion is depicted here.

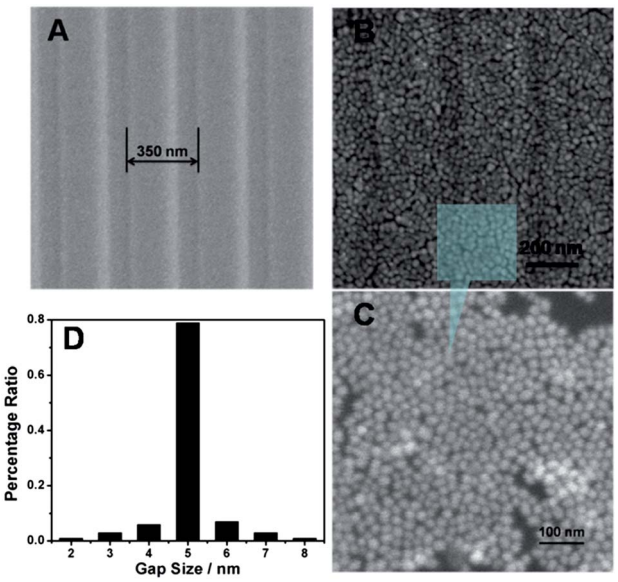


Fig. 1 (A) SEM image of Ag grating with a 350 nm period. (B) SEM image of Au NPs distributed on Ag grating. (C) SEM image of Au NPs distributed on Si wafer. (D) Statistical analysis of the gap size distributions of Au NPs.

nanoparticle and the metal film, we studied the effect of $MoO_3$ thickness on the SERS enhancement by fabricating four substrates with $MoO_3$ spacers of different thickness (2 nm, 15 nm, 35 nm, 70 nm.)

After placing the $MoO_3$ film onto the surface of Ag grating, we considered the placement of Au NPs onto the surface of $MoO_3$ covered Ag grating. Here, we conducted our own simple and versatile nanoscale force induced gold nanoparticle assembly approach to form the ordered monolayer Au NPs array (see Fig. 1C).[28] In fact, if we cannot find an effective way to uniformly arrange the Au NPs on the top of the grating, we will encounter many problems, especially in SERS measurement such as poor reproducibility of the SERS-active sites. Because LSPR is highly dependent on the spacing between nanoparticles, a nanoparticle array with uniform shape and size distribution provides the largest SERS enhancement. Fig. 1B shows the SEM image of the as-proposed Au NPs–Ag grating coupling system after a monolayer of Au NPs array was fabricated by our own self-assembly method on the top of the $MoO_3$ spacer. The Au NPs (25 nm) on the Ag grating surface were distributed compactly and uniformly, which shows them to be a promising substrate for highly-reproducible SERS detections. Especially, the inter-particle gap (about 5 nm, which was clearly revealed by the statistical analysis of the gap size distribution, as shown in Fig. 1D, more details can be seen in Fig. S1†) is very small, which will be beneficial for the NP–NP coupling to generate a huge plasmonic enhancement. Since there are four gratings with different spacer thickness, we obtained four kinds of double resonance substrates. Hereinafter, we name the double resonance substrate using grating with a 2 nm thick $MoO_3$ spacer as sample 1, the substrate using grating with 15 nm, 35 nm, 70 nm thick $MoO_3$ spacer as sample 2, sample 3, and sample 4, respectively. The Au NPs of the fabricated device were spheres with a diameter of 25 nm and a period of 30 nm. The silver film was 100 nm thick. The thickness of the $MoO_3$ spacer was varied from 2 nm to 70 nm. The fabricated substrates were illuminated with collimated and polarized laser light at normal incidence. The polarization was parallel to one of the axes of the rectangular lattice, *i.e.* the *x* axis in Scheme 1.

## SERS measurements

To evaluate the sensitivity of the SERS performance of the double resonance substrates, SERS experiments were conducted using CV as the target molecule due to its well-established vibrational features. We first studied the effect of the thickness of $MoO_3$ on SERS performance. After obtaining the optimized thickness of $MoO_3$, we evaluated the SERS enhancement performance by comparing the double SERS substrate (Au NPs/$MoO_3$/Ag grating) with the single SERS substrate, including Ag grating and Au NPs. Fig. 2 shows the SERS sensitivity measurement obtained from the double resonance substrates treated in a series of CV with 633 nm excitation. The Raman bands at about 422, 804, 913, 1174, 1368, and 1620 $cm^{-1}$ can be attributed to CV and agreed well with the reported literature.[32] With a decreasing CV concentration, the intensity of the Raman peaks gradually weakened. Raman peaks can be obtained even in $10^{-9}$ M of CV, which implies that the double resonance substrates can maintain its sensitivity for SERS detection when the concentration of CV is greater than $10^{-9}$ M. It displays an outstanding SERS sensitivity of the substrates. Furthermore, we studied the enhancement of the four Au NPs–Ag grating coupling system with different $MoO_3$ thickness by calculating their enhancement factor (EF) (see Table 1).[33–37] Assuming that the excitation volume in the form of a cylinder, the diameter (d) and the height (*h*) of the laser spot were determined by the following equations:

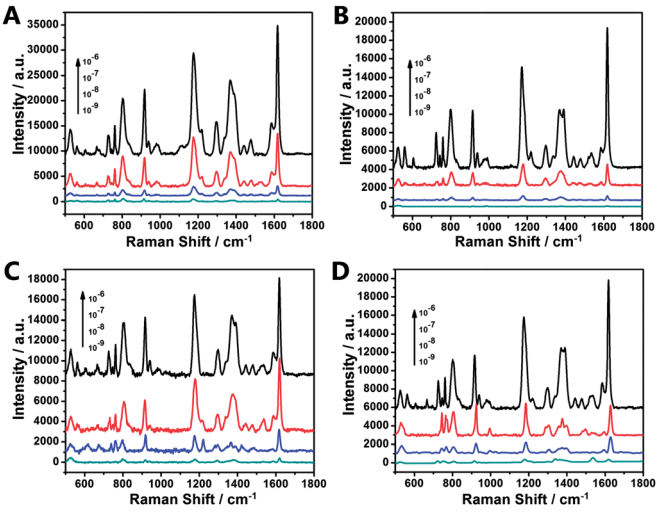


Fig. 2 The SERS spectra of different concentrations of CV solution collected on (A) sample 1, (B) sample 2, (C) sample 3, (D) sample 4.

Table 1 Calculated SERS enhancement factors for double resonance substrates and Au NPs arrays substrate

| Substrate | Sample 1 | Sample 2 | Sample 3 | Sample 4 | Ag grating | Au NPs |
|---|---|---|---|---|---|---|
| EF | $2.47 \times 10^7$ | $1.36 \times 10^7$ | $9.44 \times 10^6$ | $1.29 \times 10^7$ | $6.58 \times 10^6$ | $2.44 \times 10^6$ |

$$d = \frac{1.22\lambda_{laser}}{NA} = 1.54\ \mu m \quad (1)$$

$$h = \frac{2.2n\lambda_{laser}}{\pi(NA)^2} = 2.89\ \mu m \quad (2)$$

where $\lambda_{laser}$ is the wavelength of the laser ($\lambda_{laser}$ = 633 nm), Numerical Aperture (NA) = 0.5, $n$ is the refractive index of neat CV crystal powder ($n \approx 1.63$). The absolute magnitude of the EF for reversible hotspots was estimated according to the following equation:

$$EF = \frac{I_{SERS}/N_{SERS}}{I_{bulk}/N_{bulk}} \quad (3)$$

where $I_{SERS}$ and $I_{bulk}$ denote the Raman scattering intensities from the CV adsorbed on the surface of double resonance substrates and the solid CV, respectively; $N_{SERS}$ and $N_{bulk}$ represent the numbers of the corresponding surface and solid molecules effectively excited by the laser beam, respectively. The number of CV molecules excited in the bulk solid, $N_{bulk}$, can be calculated by the following eqn (4):

$$N_{bulk} = \frac{\pi\left(\frac{d}{2}\right)^2 h\rho N_A}{M} \quad (4)$$

where $\rho$ and $M$ are the density and molecular weight of CV, respectively, and $N_A$ represents the Avogadro constant. In this study, the density of the solid CV was 1.19 g cm$^{-3}$ and molecular weight was 407.98 g mol$^{-1}$. The calculated value of $N_{bulk}$ was $9.45 \times 10^9$. $N_{SERS}$ is the average number of adsorbed molecules in the scattering volume for the SERS measurements. We used 5 μL of $1 \times 10^{-9}$ M CV to evaluate the enhancement factor. In this case, the CV molecules bound strongly to the Ag surface. We assumed that all the CV molecules could adsorb onto the surface of the substrate, and all the CV molecules were uniformly distributed over the surface. The diameter ($D$) of the substrate square piece was 2 mm, while the diameter ($d$) of the laser spot was 1.54 μm (eqn (1)). Therefore, $N_{SERS}$ was estimated to be about $10^3$.

The study must be conducted under identical experimental conditions (laser wavelength, laser power, microscope objective or lenses, spectrometer, *etc.*), and the same preparation conditions. Based on the intensity at 1620 cm$^{-1}$, we found that sample 1 with 2 nm $MoO_3$ thickness shows the strongest Raman enhancement. Moreover, the calculated EF factor for grating should be orders of magnitude smaller than the SERS enhancement from particle arrays. The larger SERS observed experimentally on grating could be caused by the rough surfaces of the grating caused by thermal evaporation.

In addition to studying the effect of $MoO_3$ thickness on the Au NPs–Ag grating coupling system, we also compared SERS signals obtained from the double plasmonic structure (Au NPs–Ag grating coupling system) to the single Ag grating or single Au NPs structure exhibiting single resonance. Fig. 3A shows the SERS spectra obtained from the samples (Ag grating, Au NPs array, sample 1, sample 2, sample 3, sample 4) treated in $1 \times 10^{-6}$ M CV with 633 nm excitation. It can be found that the SERS signals of CV obtained from double resonance substrates are all stronger than that obtained from single resonance substrates, and sample 1 has the highest response. The SERS enhancement intensity from sample 1 at 1620 cm$^{-1}$ (about 26 000) is 11 times stronger than that of Au NPs (about 2300), which gives the weakest enhancement. The SERS spectra obtained from the samples treated in $1 \times 10^{-7}$, $1 \times 10^{-8}$, and $1 \times 10^{-9}$ M CV demonstrated the same outcome, as shown in Fig. 3A. The SERS signal obtained from composite substrates exhibiting double resonance behavior are all stronger than that obtained from Au NPs exhibiting single resonance, and sample 1, the substrate with a spacer thickness of 2 nm, shows the highest enhancement. As shown in Table 1, the double resonance structures can provide an enhancement roughly 11 times larger than the single resonance only "Au NPs array" structures. The experimental EF reaches $2.47 \times 10^7$, which is one of the highest reported in the double-resonance system to date. The very strong near-field produced in the proposed SERS substrates is due to multiple couplings, including the Au NPs–Ag grating film coupling and Au NPs–Au NPs coupling (will be discussed by theoretical modelling later). In addition, to the best of our knowledge, the Ag grating showing clear SPP effect is used for the first time in the double-resonance system, and the monolayer Au NPs array

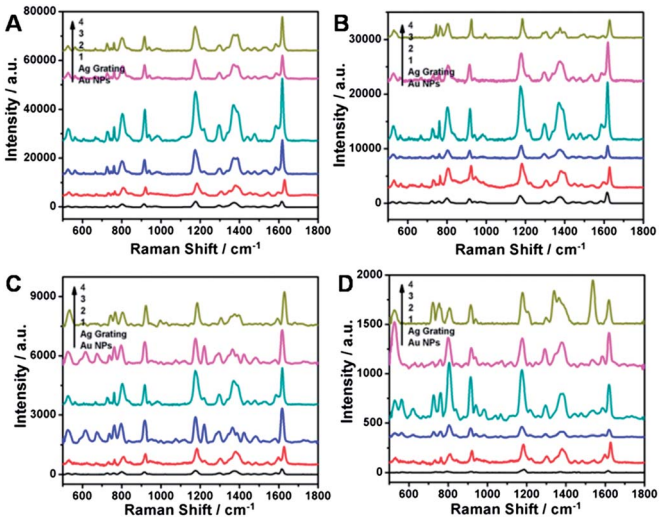


Fig. 3 SERS spectra of (A) $1 \times 10^{-6}$ M, (B) $1 \times 10^{-7}$ M, (C) $1 \times 10^{-8}$ M, (D) $1 \times 10^{-9}$ M CV molecules obtained from sample 1, sample 2, sample 3, sample 4, Ag grating and Au NPs array substrates.

is well assembled onto the top of the Ag grating with a compact and uniform distribution. Although a previous study on NPs–planar film system achieved great success, limitations in achieving double-resonance SERS system through the strategic assembly of Au NPs spaced by a $MoO_3$ nanospacer from an Ag grating film still exist. Our current study of a very simple and versatile nanoscale force induced gold nanoparticle assembly approach to form the ordered monolayer Au NPs array on the top of grating surface can directly address these issues. As a result, the results clearly indicate that the Au NPs–Ag grating coupling system with a 2 nm $MoO_3$ spacer dramatically boosts the intensity of Raman scattering and therefore, has the potential to become a powerful tool in analytical science and related fields.

Why does sample 1 substrate show the highest SERS enhancement? As shown in Scheme 2, a surface plasmon is a quantum of an electron concentration wave that can exist at a dielectric–metal interface. The surface plasmon propagates along the metal surface and decays exponentially into both the media. Thus, the excited surface plasmons from the Ag surface can be transferred to the top metal (Au) surface through the dielectric layer. The thinner the dielectric layer is, the less the surface plasmon decays. Accordingly, the conduction electrons on the Au surface are further localized.

### FDTD simulations

To better understand the nature of the strong near-field enhancement in the Au NPs–Ag grating coupling system, we conducted a theoretical study utilizing the finite-difference time-domain (FDTD) method on the system in which the optical interactions between Au NPs themselves as well as between Au NPs and Ag grating were fully considered. In the modeling, the sample geometries closely matched those of the actual experimental samples, *i.e.*, a 25 nm Au NP on an Ag grating with a 350 nm period separated by different thicknesses of $MoO_3$ spacer (2 nm, 15 nm, 35 nm, 70 nm). The gap between the neighboring Au NPs was about 5 nm. We first simulated the near field spectra for the single resonance and double resonance structure. Fig. 4 shows the cross-section near field profiles of TM polarized light at 633 nm for different metal structures: (a) Au NPs–Au NPs coupling with 5 nm, (b) single Ag grating, (c) double-resonance Au NP/$MoO_3$/Ag grating and (d) partial enlargement of Au NP/$MoO_3$/Ag grating. For the Au NPs array

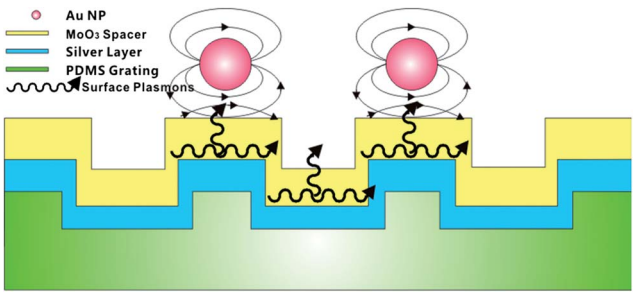


Scheme 2 Schematic of the fabricated double resonance substrate showing high SERS enhancement.

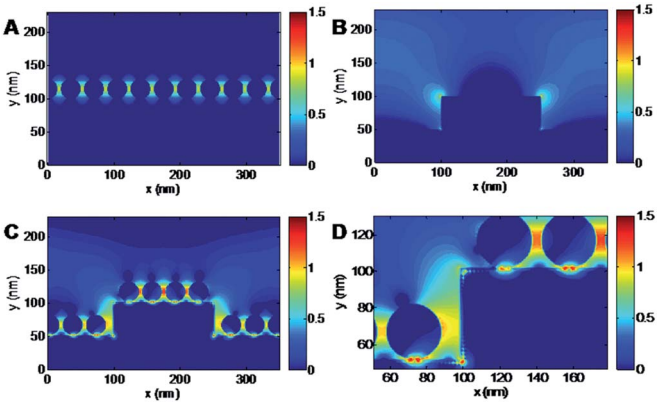


Fig. 4 The cross-section near field profiles of TM polarized light at 633 nm for different metal structures: (A) Au NPs–NPs coupling with 5 nm, (B) single Ag grating and (C) double-resonance Au NP/$MoO_3$/Ag grating, (D) partial enlargement of Au NP/$MoO_3$/Ag grating.

structure, we found a (plasmonic-induced) strong near-field with a local enhancement factor (EF) of $9.21 \times 10^6$ where EF is approximately defined as $|E_{local}/E_0|^4$. The strong near field located at the NP–NP gap is caused by the strong plasmonic coupling (Fig. 4A). In contrast, for the single Ag grating structure, the evanescent field above the Ag grating indicates the excitation of the SPP mode at the interface of the Ag film and the $MoO_3$ spacer (Fig. 4B) and the local EF is $5.24 \times 10^7$. For the Au NP/$MoO_3$/Ag grating double-resonance structure, enhanced near fields in the vicinity of the Au NPs can be seen (Fig. 4C and D) but with the addition of an extended evanescent field above the Ag grating, which is characteristic of the SPP. These results indicate that the two resonances for strong coupling case carry both the characteristics of LSPs and SPPs, and finally the local EF reaches $8.38 \times 10^8$.

Then, we simulated the cross-section near field profiles for double-resonance Au NP/$MoO_3$/Ag grating structure with different thickness of $MoO_3$, as shown in Fig. 5. It can be seen that enhanced near fields exist around the gold nanoparticles

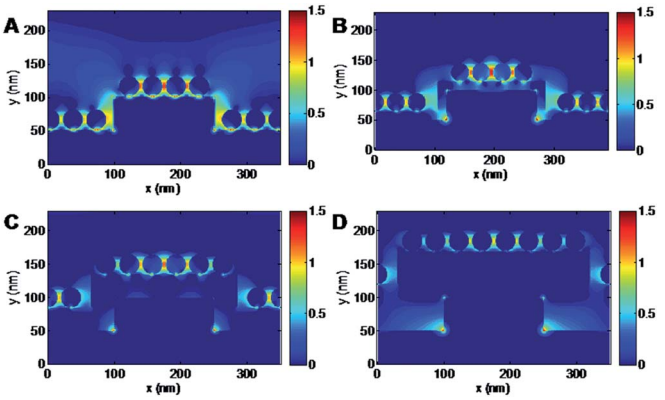


Fig. 5 The cross-section near field profiles of TM polarized light at 633 nm for double-resonance Au NP/$MoO_3$/Ag grating structure with different thickness of $MoO_3$: (A) 2 nm, (B) 15 nm, (C) 35 nm, and (D) 70 nm.

and an extended evanescent field is above the Ag grating. We observed that the Au NP/$MoO_3$/Ag grating structure with a 2 nm thick $MoO_3$ shows the highest field enhancement. We also observed that the stronger plasmonic enhancement is, the smaller the thickness of $MoO_3$ spacer between the upper Au NPs and lower Ag grating is. Our result is consistent with the previous report that the local field enhancement of hot spots is critically sensitive to the nanoscale spacer between the NP and the film.[38]

As a consequence, our experimental and theoretical results reveal a greater field enhancement for Au NPs–Ag grating coupling system due to the multiple couplings including Au NPs–Au NPs coupling and Au NPs–Ag grating coupling, which will play a very important role in the Au NPs–Ag grating system. On one hand, the multiple couplings considerably strengthen the near-field. Thus an enormous EF of $2.47 \times 10^7$ has been achieved. On the other hand, the very strong field enhancement at system can also offer a unique opportunity in highly sensitive analyte characterization.

### Reproducibility of SERS detection

When employing SERS technology, the reproducibility of SERS substrates should be taken into account. The relative standard deviation (RSD) of major peaks is often used to estimate the reproducibility of SERS signals. The main Raman vibrations of CV at 1174, 1368, and 1620 $cm^{-1}$ were obviously enhanced at all the spots indicating excellent SERS activity and reproducibility. Fig. 6 shows the SERS-RSD spectrum of CV molecules randomly collected from 50 positions of sample 1. The RSD of the Raman vibrations from sample 1 at 1174, 1368, and 1620 $cm^{-1}$ are 14.94, 13.54, and 14.96%, respectively. The maximal RSD value of signal intensities of major SERS peaks was observed to be below 0.2, indicating that the double resonance substrate has good reproducibility across the entire area.[39] The compact and uniform distribution of Au NPs on the Ag grating surface is the reason why the double resonance substrate shows highly reproducible SERS detection.

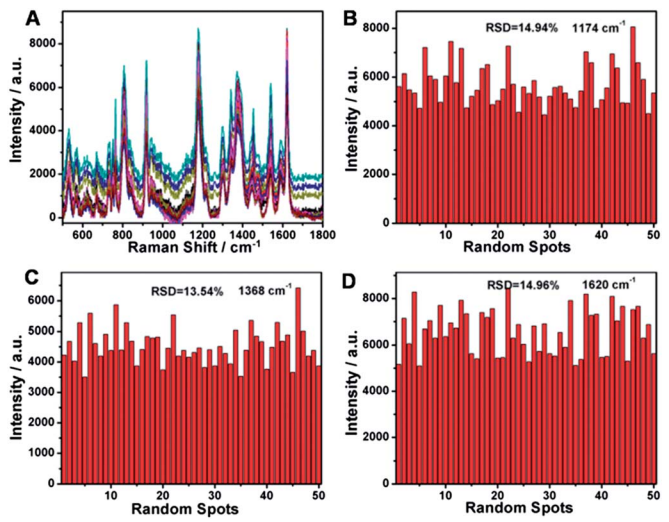


Fig. 6 (A) Series of SERS spectra of $10^{-6}$ M CV collected randomly from 50 spots of sample 1. (B), (C) and (D) are the intensities of the main vibrations of $10^{-6}$ M CV at 1174, 1368 and 1620 $cm^{-1}$.

## Conclusions

We proposed a novel NPs–film coupling system by introducing Ag grating into this system. Our results show that the Au NPs–Ag grating coupling system offers tremendous near-field enhancements with one of the highest enhancement ratio ($2.47 \times 10^7$) reported to date in the NPs–film coupling system. The Ag grating showing clear SPP effect is used for the first time in the double-resonance system, and the monolayer Au NPs array is well assembled onto the top of the Ag grating with a compact and uniform distribution (inter-particles gap about 5 nm). Our experimental and theoretical results show that the enhancement can be explained by the multiple couplings between the Ag NPs as well as between the Ag film and Ag NPs. By studying the organic dye CV as an analyte, we show that the as-proposed Au NPs–Ag grating coupling system can be used to realize the sensitive detection of most environmental pollutants. Furthermore, we strongly believe that this simple and reliable method would offer a stepping stone in enabling quantitative plasmonic sensing at the single molecule level. Our results show that the proposed system can function as a powerful tool in analytical science and related fields.

## Notes and references

1 D. L. Jeanmaire and R. P. Van Duyne, *J. Electroanal. Chem.*, 1977, **84**, 1–20.
2 M. G. Albrecht and J. A. Creighton, *J. Am. Chem. Soc.*, 1977, **99**, 5215–5217.
3 K. Kneipp, M. Moskovits and H. Kneipp, *Surface-enhanced Raman scattering: physics and applications*, Springer, NewYork, 2006.
4 A. Campion and P. Kambhampati, *Chem. Soc. Rev.*, 1998, **27**, 241–250.
5 C. L. Haynes, A. D. McFarland and R. P. Van Duyne, *Anal. Chem.*, 2005, **77**, 338A–346A.
6 P. L. Stiles, J. A. Dieringer, N. C. Shah and R. R. Van Duyne, *Annu. Rev. Anal. Chem.*, 2008, **1**, 601–626.
7 M. Moskovits, *Rev. Mod. Phys.*, 1985, **57**, 783–826.
8 S. A. Maier, *Plasmonics: Fundamentals and Applications: Fundamentals and Applications*, Springer, 2007.
9 K. L. Kelly, E. Coronado, L. L. Zhao and G. C. Schatz, *J. Phys. Chem. B*, 2003, **107**, 668–677.
10 K. Kneipp, Y. Wang, H. Kneipp, L. T. Perelman, I. Itzkan, R. R. Dasari and M. S. Feld, *Phys. Rev. Lett.*, 1997, **78**, 1667–1670.
11 K. Kneipp, H. Kneipp, I. Itzkan, R. R. Dasari and M. S. Feld, *J. Phys.: Condens. Matter*, 2002, **14**, R597–R624.
12 A. D. McFarland, M. A. Young, J. A. Dieringer and R. P. Van Duyne, *J. Phys. Chem. B*, 2005, **109**, 11279–11285.
13 C. E. Talley, J. B. Jackson, C. Oubre, N. K. Grady, C. W. Hollars, S. M. Lane, T. R. Huser, P. Nordlander and N. J. Halas, *Nano Lett.*, 2005, **5**, 1569–1574.

 

14 T. H. Reilly, S. H. Chang, J. D. Corbman, G. C. Schatz and K. L. Rowlen, *J. Phys. Chem. C*, 2007, **111**, 1689–1694.
15 C. L. Haynes, A. D. McFarland and R. P. Van Duyne, *Anal. Chem.*, 2005, **77**, 338A–346A.
16 H. X. Xu, E. J. Bjerneld, M. Käll and L. Börjesson, *Phys. Rev. Lett.*, 1999, **83**, 4357–4360.
17 H. X. Xu, J. Aizpurua, M. Käll and P. Apell, *Phys. Rev. E: Stat. Phys., Plasmas, Fluids, Relat. Interdiscip. Top.*, 2000, **62**, 4318–4324.
18 M. Kahl and E. Voges, *Phys. Rev. B: Condens. Matter Mater. Phys.*, 2000, **61**, 14078–14088.
19 N. Papanikolaou, *Phys. Rev. B: Condens. Matter Mater. Phys.*, 2007, **75**, 235426.
20 A. Ghoshal and P. G. Kik, *J. Appl. Phys.*, 2008, **103**, 113111.
21 Y. Z. Chu and K. B. Crozier, *IEEE Lasers and Electro-Optics Society*, 2008, 492–493.
22 Y. Z. Chu and K. B. Crozier, *Opt. Lett.*, 2009, **34**, 244–246.
23 Y. Z. Chu, M. G. Banaee and K. B. Crozier, *ACS Nano*, 2010, **4**, 2804–2810.
24 M. G. Banaee and K. B. Crozier, *ACS Nano*, 2011, **5**, 307–314.
25 A. Q. Chen, R. L. Miller, A. E. DePrince, III, A. Joshi-Imre, E. Shevchenko, L. E. Ocola, S. K. Gray, U. Welp and V. K. Vlasko-Vlasov, *Small*, 2013, **9**, 1939–1946.
26 D. X. Wang, W. Q. Zhu, Y. Z. Chu and K. B. Crozier, *Adv. Mater.*, 2012, **24**, 4376–4380.
27 G. Frens, *Nature (London), Phys. Sci.*, 1973, **241**, 20–22.
28 X. Zhou, F. Zhou, H. L. Liu, L. B. Yang and J. H. Liu, *Analyst*, 2013, **138**, 5832–5838.
29 X. G. Ren, Z. X. Huang, X. L. Wu, S. L. Lu, H. Wang, L. Wu and S. Li, *Comput. Phys. Commun.*, 2012, **183**, 1192–1200.
30 A. Taflove and S. C. Hagness, *Computational electromagnetics: the finite-difference time-domain method*, Artech House, Boston, 2005.
31 P. B. Johnson and R. W. Christy, *Phys. Rev. B: Condens. Matter Mater. Phys.*, 1972, **6**, 4370–4379.
32 M. V. Canamares, C. Chenal, R. L. Birke and J. R. Lombardi, *J. Phys. Chem. C*, 2008, **112**, 20295–20300.
33 G. Hong, C. Li and L. Qi, *Adv. Funct. Mater.*, 2010, **20**, 3774–3783.
34 E. C. Le Ru, E. Blackie, M. Meyer and P. G. Etchegoin, *J. Phys. Chem. C*, 2007, **111**, 13794–13803.
35 X. M. Lin, Y. Cui, Y. H. Xu, B. Ren and Z. Q. Tian, *Anal. Bioanal. Chem.*, 2009, **394**, 1729–1745.
36 S. Tian, Q. Zhou, Z. Gu, X. Gu and J. Zheng, *Analyst*, 2013, **138**, 2604–2612.
37 H. L. Liu, Y. D. Sun, Z. Jin, L. B. Yang and J. H. Liu, *Chem. Sci.*, 2013, **4**, 3490–3496.
38 C. Ciraci, R. T. Hill, J. J. Mock, Y. Urzhumov, A. I. Fernandez-Dominguez, S. A. Maier, J. B. Pendry, A. Chilkoti and D. R. Smith, *Science*, 2012, **337**, 1072–1074.
39 B. H. Zhang, H. S. Wang, L. H. Lu, K. L. Ai, G. Zhang and X. L. Cheng, *Adv. Funct. Mater.*, 2008, **18**, 2348–2355.